



Hierarchical Rules for Argonaute Loading in *Drosophila*

Citation

Czech, Benjamin, Rui Zhou, Yaniv Erlich, Julius Brennecke, Richard Binari, Christians Villalta, Assaf Gordon, Norbert Perrimon, and Gregory J. Hannon. "Hierarchical rules for Argonaute loading in *Drosophila*." *Molecular Cell* 36, no. 3 (2009): 445-456.

Permanent link

<https://nrs.harvard.edu/URN-3:HUL.INSTREPOS:37367164>

Terms of Use

This article was downloaded from Harvard University's DASH repository, and is made available under the terms and conditions applicable to Other Posted Material, as set forth at <http://nrs.harvard.edu/urn-3:HUL.InstRepos:dash.current.terms-of-use#LAA>

Share Your Story

The Harvard community has made this article openly available.
Please share how this access benefits you. [Submit a story](#).

[Accessibility](#)

Published in final edited form as:

Mol Cell. 2009 November 13; 36(3): 445–456. doi:10.1016/j.molcel.2009.09.028.

Hierarchical rules for Argonaute loading in *Drosophila*

Benjamin Czech^{1,*}, Rui Zhou^{2,*}, Yaniv Erlich¹, Julius Brennecke^{1,3}, Richard Binari², Christians Villalta², Assaf Gordon¹, Norbert Perrimon^{2,#}, and Gregory J. Hannon^{1,#}

¹Watson School of Biological Sciences Howard Hughes Medical Institute Cold Spring Harbor Laboratory 1 Bungtown Road Cold Spring Harbor, NY 11724, USA

²Harvard Medical School Department of Genetics Howard Hughes Medical Institute 77 Avenue Louis Pasteur Boston, MA 02115, USA

Summary

Drosophila Argonaute-1 and Argonaute-2 differ in function and small RNA content. AGO2 binds to siRNAs, whereas AGO1 is almost exclusively occupied by microRNAs. MicroRNA duplexes are intrinsically asymmetric, with one strand, the miR strand, preferentially entering AGO1 to recognize and regulate the expression of target mRNAs. The other strand, miR*, has been viewed as a byproduct of microRNA biogenesis. Here, we show that miR*s are often loaded as functional species into AGO2. This indicates that each microRNA precursor can potentially produce two mature small RNA strands that are differentially sorted within the RNAi pathway. miR* biogenesis depends upon the canonical microRNA pathway, but loading into AGO2 is mediated by factors traditionally dedicated to siRNAs. By inferring and validating hierarchical rules that predict differential AGO loading, we find that intrinsic determinants, including structural and thermodynamic properties of the processed duplex, regulate the fate of each RNA strand within the RNAi pathway.

Keywords

Drosophila melanogaster; microRNA; AGO2; endo-siRNAs; small RNA sorting

Introduction

The biogenesis of small RNAs derived from double-stranded or structured precursors requires the action of RNase III family proteins. In *Drosophila*, these small RNAs interact with the two AGO clade proteins, Argonaute-1 (AGO1) and Argonaute-2 (AGO2), and represent two major classes, microRNAs (miRNAs) and small interfering RNAs (siRNAs), respectively.

Small interfering RNAs (siRNAs) are processed from exogenous dsRNAs by a dedicated Dicer protein, Dcr-2, and its cofactor, R2D2 (Lee et al., 2004b; Liu et al., 2003). Dcr-2 and R2D2 additionally function during siRNA loading into AGO2 (Tomari et al., 2004). In a mature complex, only one siRNA strand, the guide strand, is retained. The remaining strand, the

© 2009 Elsevier Inc. All rights reserved.

#To whom correspondence should be addressed (hannon@cshl.edu; perrimon@receptor.med.harvard.edu).

³current address: IMBA - Institute of Molecular Biotechnology Dr. Bohr-Gasse 3 1030 Vienna, Austria

*These authors contributed equally to this work

Publisher's Disclaimer: This is a PDF file of an unedited manuscript that has been accepted for publication. As a service to our customers we are providing this early version of the manuscript. The manuscript will undergo copyediting, typesetting, and review of the resulting proof before it is published in its final citable form. Please note that during the production process errors may be discovered which could affect the content, and all legal disclaimers that apply to the journal pertain.

passenger strand, is cleaved by AGO2 and ultimately degraded (Matranga et al., 2005; Miyoshi et al., 2005).

Endogenously encoded double-stranded RNAs can also form siRNAs, endosRNAs (Czech et al., 2008; Ghildiyal et al., 2008; Kawamura et al., 2008; Okamura et al., 2008a). These can be derived from dedicated non-coding transcripts that are extensively structured, from intermolecular hybrids of RNAs from convergently transcribed genes, or from transposon loci, which form dsRNA through unknown mechanisms. Endo-siRNAs are processed by Dcr-2 but lack a strong dependency on R2D2 (Czech et al., 2008; Okamura et al., 2008a). Instead, they rely upon a specific isoform of the dsRNA binding protein, Loquacious (Loqs-PD) (Czech et al., 2008; Hartig et al., 2009; Okamura et al., 2008a; Zhou et al., 2009). Both endo- and exo-siRNA primed AGO2 execute efficient small RNA-directed cleavage of complementary targets (Czech et al., 2008; Hammond et al., 2000). Moreover, all AGO2-bound guide strands become 2'-O-methyl modified at their 3' termini by the methyltransferase, Hen1/Pimet (Horwich et al., 2007; Saito et al., 2007).

In contrast to AGO2, AGO1 principally hosts microRNAs. These are derived mainly from long RNA polymerase II transcripts through two site-specific cleavages. The first is catalyzed by Drosha/Pasha complexes (Denli et al., 2004; Gregory et al., 2004; Lee et al., 2003; Lee et al., 2004a) and the second by Dcr-1 in collaboration with another Loquacious isoform, Loqs-PB (Forstemann et al., 2005; Jiang et al., 2005; Park et al., 2007; Saito et al., 2005). The product of Dcr-1 cleavage is a duplex comprised of the miRNA (miR) and the miRNA-star (miR*) strands, with the miR corresponding to the guide strand, and the miR* resembling the passenger strand. Loading of these duplexes into AGO1 followed by unwinding and degradation of the miR* strand leads to mature RISC. The miR strand guides AGO1 to mRNA targets, which are generally recognized by imperfect base-pairing interactions. Recognition by microRNAs generally leads to repression via reduction in protein synthesis. Although both AGO1 and AGO2 can act via this mechanism (Forstemann et al., 2007; Iwasaki et al., 2009), AGO1 seems biochemically optimized for cleavage-independent repression, while AGO2 is optimized as a multi-turnover nuclease (Forstemann et al., 2007).

Based upon these observations, small RNAs in the RNAi pathway must be sorted in several ways. First, different types of small RNA duplexes are directed toward specific AGO complexes. Second, the individual strands of each small RNA duplex have a different probability of guiding mature RISC. As a consequence of coupled dicing and loading, selective incorporation into AGO1 or AGO2 could rely in part on the distinct enzymatic machinery underlying the biogenesis of siRNAs and microRNAs. However, at least one microRNA, *miR-277*, is substantially AGO2 loaded, although it is processed conventionally by Dcr-1 and Loqs (Forstemann et al., 2007). In contrast to many miRNA precursors, which contain several mismatches and bulges, the duplex precursor to *miR-277* has an unusual degree of perfect double-stranded character, and therefore strongly resembles a siRNA precursor. Moreover alterations in the extent of pairing in microRNA-mimetic siRNA duplexes allowed experimental direction to AGO1 or AGO2 preferentially (Tomari et al., 2007). The discrimination of miR and guide strands from miR* and passenger strands is proposed to rely upon the thermodynamic properties of the processed duplexes. In both cases, the strand with the less stable 5' end preferentially enters RISC.

Conventional wisdom holds that the passenger and miR* strands are simply by-products of siRNA and miRNA biogenesis and RISC loading and are, therefore, discarded and degraded. However, in our studies of AGO2-bound small RNA species we noted that a wide range of miR* strands represented some of the most abundant individual species in AGO2 RISC. This indicated that following processing by Dcr-1, the miR:miR* duplex could be bi-functional, flowing down either the AGO1 or AGO2 loading pathway with the properties of each

individual strand determining its destination. By studying the patterns of mismatches and thermodynamic stabilities of precursors to small RNAs resident within each complex and by selectively manipulating these characteristics, we find that a hierarchy of rules, depending both on duplex structure and thermodynamic properties, determine the fate of small RNAs in the RNAi pathway.

Results

miR* strands often bear 2'-O-methylated 3' termini

We sought to investigate the fates of dsRNA-derived small RNAs and their flow through the RNAi pathway. We began by sequencing a 19- to 24-nt small RNA library from wild-type *Drosophila* S2 cells using our standard cloning protocol (“standard”; Fig. 1). In parallel, we analyzed a library enriched for small RNAs with 2'-O-methylated 3' termini (“oxidized”) prepared using a modified cloning strategy (Seitz et al., 2008). After removing degradation products of abundant cellular RNAs, sequences were split into six categories: endo-siRNAs corresponding to (1) genes, (2) structured loci, (3) repeats, (4) viruses, and (5) genomic regions without annotation (“none”), and (6) microRNA (miR or miR*). 62.6% of all sequences within the standard library fell within different endo-siRNA classes. The remaining 37.4% corresponded to miRNA sequences, of which the vast majority derived from mature miRNA strands (Fig. 1A). Consistent with previous reports that *Drosophila* miRNAs lack methylated 3' termini (Horwich et al., 2007; Saito et al., 2007), miRNA species were significantly depleted in the oxidized library. There, 97.7% reads could be assigned endo-siRNAs, while only 2.3% corresponded to miRNA sequences. Within the remaining miRNA sequences, mature miRNA strands were strongly depleted, while levels of miRNA* strands did not change substantially. Specifically, ratios between miR and miR* strands changed from ~33:1 in the standard library to ~2:1 in the oxidized library, which corresponds to a 16-fold relative enrichment of miR*. Consistent with previous reports of siRNAs derived from the flock house virus (FHV) being only partially methylated (Aliyari et al., 2008; Flynt et al., 2009), viral siRNAs (more than 99% of our viral siRNAs matched to the FHV genome) were also reduced in the oxidized library. All other categories of endo-siRNAs were enriched by the modified cloning strategy (Fig. 1A), consistent with the RNAs bearing modified 3' termini (Chung et al., 2008; Kawamura et al., 2008; Okamura et al., 2008a). We plotted the cloning frequencies of the 40 most abundant sequences in each library corresponding to miRs (red text), miR*s (blue text) and endo-siRNAs from structured loci (black text) (Fig. 1B). We calculated the relative representation of each sequence in the two libraries and sorted by this ratio. Green bars indicate enrichment in the standard library and red bars indicate enrichment in the oxidized library. Since 2'-O-methylation is characteristic of AGO2-loaded sequences, this ratio can also be taken as a rough surrogate for relative loading into AGO1 and AGO2 complexes. The results of this analysis are consistent with previous reports of microRNAs principally occupying AGO1 and endo-siRNAs occupying AGO2 (Fig. 1B). Notably, these data also indicated that miR* strands were individually abundant within AGO2 complexes.

miR* strands primarily associate with AGO2

To confirm the patterns of small RNA loading, we examined small RNA libraries from immunoprecipitates of AGO1 and AGO2 from *Drosophila* S2 cells (Czech et al., 2008), separating miRNA-related sequences into miR and miR* strands. ~98% of all AGO1-associated reads match to annotated miRNAs, with 99% of these representing the miR strand. In contrast to recent reports, we did not observe significant loading of miR*s into AGO1 (Okamura et al., 2008b). The remaining AGO1-associated sequences comprised distinct classes of endo-siRNAs including genic and viral sequences (Fig. 2A). In contrast, AGO2 is predominantly loaded with all classes of endo-siRNAs. Approximately 8% of all reads in AGO2 immunoprecipitates match to miRNAs. Among the AGO2-associated miRNA

sequences, only ~40% matched to the miR strand, while almost 60% represented miR* strands (Fig. 2A).

To verify conclusions emerging from deep sequencing, we prepared total RNA from AGO1 and FLAG immunoprecipitates from a stable S2 line expressing FLAG/HA-AGO2 under its endogenous regulatory elements (Czech et al., 2008) (Supplementary Fig. 1A) and subjected a fraction of this material to β -elimination. Treated and untreated RNAs were blotted with probes specific to the miR and miR* strands of three microRNAs, *miR-bantam*, *miR-184* and *miR-276a*. miR-strand probes for all three miRNAs generated strong signals in AGO1 immunoprecipitates and were only weakly, if at all, detected in AGO2 immunoprecipitates (Fig. 2B). In contrast, all three miR* probes detected strong signals selectively in AGO2 immunoprecipitates. As expected, the endo-siRNA, *esi-2.1*, strongly associated with AGO2 (Czech et al., 2008). RNAs co-immunoprecipitated with AGO1 were sensitive to periodate treatment followed by β -elimination. However, all AGO2-associated RNAs including the low abundance AGO2-associated miR strands were completely resistant to β -elimination (Fig. 2B).

Patterns observed by Northern blotting were also apparent in an analysis of the most abundant sequences derived from AGO1 and AGO2 complexes (Fig. 2C). In AGO1 complexes, miR strands (red text) were strongly enriched, whereas miR*s (blue text) and endo-siRNAs (black text) were rare. In AGO2, miR*s and endo-siRNAs were cloned at higher frequencies. Consistent with a previous report (Forstemann et al., 2007), we also observed a significant proportion of *miR-277* in AGO2.

Our data imply that AGO1 and AGO2 loading rests on a more complex set of parameters than was previously supposed (Forstemann et al., 2007; Tomari et al., 2007). We therefore analyzed the properties of sequences that showed strong preferential (>70%) association with either AGO1 or AGO2 (Fig. 2D,E). We assessed overall base-pairing patterns and the distributions of mismatches within miR:miR* and endo-siRNA guide:passenger duplexes and determined their positional nucleotide biases. In general, duplexes sorted to AGO1 contained slightly higher frequencies of mismatched bases than those sorted to AGO2, indicating that overall pairing is a minor determinant of small RNA sorting. Nucleotide biases were prominent for AGO1-loaded RNAs, with the previously noted strong enrichment for a 5' U in microRNAs being easily observed (Fig 2D). Most of either AGO1- or AGO2-destined duplexes showed standard Watson-Crick base pairs across their first two residues with rates reaching 80% for AGO2 but only 60% for AGO1 (Fig. 2D,E). In AGO2 bound RNAs, there was an enrichment for a terminal C residue (~50% of sequences).

Strong differences were detected in the structure of the central regions of duplexes sorted to AGO1 and AGO2. In particular the strand destined for AGO1 was often unpaired at position 9, while pairing at this position occurred in more than 90% of AGO2-associated strands. This pattern not only held for miR and miR* strands but also for the guide and passenger strands of endo-siRNAs. For example, both deep sequencing (not shown) and Northern Blotting (Fig. 2B) highlighted the guide strand of one endo-siRNA, *esi-2.3*, that acted anomalously, entering preferentially AGO1 rather than AGO2 complexes. Notably, in its precursor duplex, *esi-2.3* shows central mismatches characteristic of miR strands (Supplementary Fig. 2). Thus, a combination of sequence and structural determinants contribute to strand and small RNA sorting in the RNAi pathway and these characteristics dominate over signals emanating from the upstream biogenesis pathways.

Validating rules for strand sorting

To assess the relevance of our observations for small RNA strand sorting, S2 cells stably expressing FLAG/HA-AGO2 were transfected with altered *miRNA-276a* and *let-7* siRNA duplexes, and AGO1 and AGO2 complexes were subsequently recovered by

immunoprecipitation (Fig. 3A). Differential loading was probed by Northern blotting (Fig. 3B and Supplementary Fig. 3). Levels of both top (miR* for *miR-276a*, guide for *let-7*) and bottom strands (miR for *miR-276a*, passenger for *let-7*) were normalized to non-transfected controls and relative Argonaute loading indices for each strand were calculated compared to corresponding wild-type controls (Fig. 3C,D). We found that both strands of the perfectly matched *let7-1* duplex showed relatively strong association with AGO2 (Fig. 3D). The insertion of central bulges or mismatches at the ends of *let-7* duplexes caused a general shift of both top (guide) and bottom (passenger) strands towards AGO1. We observed stronger effects on AGO1 loading for the strand featuring central bulges around position 9 as measured from its 5' end (compare *let-7-4* and *let-7-7* with *let-7-2* and *let-7-3*). Introduction of mismatches at positions 9 and 10 caused a stronger preference for AGO1 loading than introduction of mismatches at positions 11 and 12 (compare the top strand with the bottom strand of *let-7-2* and *let-7-3*), in accord with our analysis of naturally AGO1-associated miRNA strands (Fig. 2D). The combination of central bulges with unpaired terminal nucleotides in reciprocal configurations caused both strands to favor AGO1 (*let-7-5*, *let-7-6*, *let-7-8*, *let-7-9*). However, the effects of central mismatches at positions 9 and 10 still showed a stronger impact than did alterations of duplex ends (compare *let-7-5* with *let-7-6*, and *let-7-8* with *let-7-9*).

Generally consistent results were obtained for sorting of *miR-276a* duplexes (Fig. 3C). Changing the 5' uracil of the miR strand (bottom, in red) to adenine did not extinguish AGO1 loading (*miR-276a-2*), while substitution of the 5' adenine of the miR* strand (top, in blue) to uracil did cause a slight shift towards AGO1 (*miR-276a-3*). Modifying the terminal nucleotides of both strands at once failed to trigger more dramatic changes in AGO preference than did single substitutions, indicating that the observed nucleotide bias of microRNAs has a minor, if any, impact on sorting behavior (*miR-276a-4*). Next we combined modification of terminal nucleotides with altered central bulges by inserting mismatches at positions 9 and 10 counted from the 5' end of either the top or bottom strands. Alteration of the miR* strand combined with reversed terminal nucleotides (*miRNA-276a-6*) caused a dramatic shift of the miR* towards AGO1, while the miR strand was moderately shifted towards AGO2. Similar results were obtained if central mismatches only were introduced into the miR* strand (*miRNA-276a-8*) or if the central mismatches were combined with mismatches in the seed region of the miR strand (*miRNA-276a-5* and *miRNA-276a-10*). Sealing the central mismatches in the miR strand either alone (*miRNA-276a-11*) or in combination with a reversion of seed mismatches (*miRNA-276a-9*) biased the miR strand towards AGO2 as compared to the wild-type duplex. Considered together, we conclude that central mismatches are the dominant determinant for sorting of small RNAs among AGO1 and AGO2 complexes, while the overall pairing within the duplex also contributes, albeit to a lesser extent. Central mismatches also contribute to the decision which strand is loaded, while thermodynamic properties become important for duplexes with relatively perfect dsRNA character.

Biogenesis of miRNA* strands

Since our results pointed to bi-functionality within microRNA precursors, we wished to compare the requirements for processing and loading of miR and miR* strands. We depleted canonical components of the miRNA and endo-siRNA pathways in S2 cells and examined the impacts on levels of miRNAs, miR*s, and endo-siRNAs derived from structured loci. RNAs from the indicated knockdowns were split and subjected to β -elimination or left untreated prior to Northern blotting. Knockdown of established microRNA pathway components generally had consistent effects on miR and miR* strands. Reduction of *drosha* and *pasha* together led to a decrease in both the miR and miR* strands, while endo-siRNA levels were not affected (Fig. 4A). Depletion of Dcr-1 caused accumulation of pre-miRNAs and slightly reduced the levels of mature miRs and miR*s, while not affecting endo-siRNAs. In contrast, knockdown

of some siRNA pathway components showed differential effects on miR and miR*. Knockdown of *dcr-2* or *loqs* had no effect on either miR or miR* levels, while endo-siRNAs were strongly reduced. However, depletion of Dcr-2 or R2D2 did cause significant band shifts for β -eliminated RNAs corresponding to miR*s. Upon AGO1 depletion, we noted a significant reduction in mature miRNA strands and an unexpected concomitant increase in the levels of *miRNA-bantam** and *miRNA-276a**. The latter resisted β -elimination, indicating proper loading into AGO2. Finally, depletion of AGO2 caused a reduction of endo-siRNA and miR* levels, while miRNA levels were unaffected. Consistent with the requirement of AGO2 binding for terminal methylation, miR*s remaining in *ago2* knockdowns had completely lost their resistance to β -elimination.

To probe the effects of AGO1 and AGO2 depletion more broadly, we sequenced small RNAs from knockdown cells (Fig. 4B). By comparing individual sequences within these libraries, we could establish relative dependence on the two AGO proteins. miR*s and endo-siRNAs showed more dependence on AGO2, whereas miRNAs were more dependent on AGO1 (Fig. 4B). We also examined the small RNA populations associated with AGO1 or AGO2 in cells depleted of Dcr-2, and observed a significant decrease in the miR* fraction within AGO2-bound miRNAs as compared to control samples (Supplementary Fig. 4). These results are consistent with miR*s being predominantly associated with AGO2 and depending upon components of the miRNA pathway for processing and components of the siRNA pathway for loading, stabilization and 3' end modification.

miR* strands can silence targets *in vitro*

miR* strands show abundances in AGO2 RISC similar to those of endo-siRNAs, which are competent to silence target RNAs (Czech et al., 2008; Okamura et al., 2008b). We therefore tested whether AGO2-loaded miR*s could repress sensors carrying perfect complementary sites. Since a recent report employed AGO2 in the regulation of bulged target sites, we also probed the impact of miR* strands on sensors carrying imperfect sites (Iwasaki et al., 2009). We generated *Renilla* luciferase reporter constructs that carry multiple perfect or bulged binding sites for either the miR or miR* strand of *miR-276a* or *miR-bantam* (Fig. 5A). These sensor constructs were transfected into S2 cells together with dsRNAs targeting canonical miRNA and siRNA pathway components, and the impact of depletion of these factors on reporter activity was examined. As expected, depletion of Drosha caused a consistent de-repression of all sensors for the miR strand of *miR-276a* or *miR-bantam*. Importantly, Drosha depletion also led to a similar de-repression of all sensors for miR* strands, indicating that these are also capable of repressing mRNA targets (Fig. 5B,C). While depletion of Pasha or Dcr-1 caused a moderate de-repression of sensors for endogenous miR or miR* strands, we observed a more consistent phenotype following over-expression of primary miRNAs (Fig. 5B–E). In addition, the sensor constructs for either *miR-276a** or *miR-bantam** in a “perfect match” configuration were de-repressed upon depletion of AGO2, consistent with their acting in a complex with this protein (Fig. 5B,C). This was dependent on Dcr-2 and R2D2, but not Loqs. Most notably, depletion of AGO1 enhanced the repression of the same set of sensors, in accord with the observed increase in miR* strands in knockdown cells (Fig. 5B,C). Similar changes in sensor activity were observed when pri-miRNAs were over-expressed (Fig. 5D,E). We therefore conclude that miR* strands are capable of silencing target transcripts carrying either perfect or imperfect complementary sites in cultured S2 cells and that the silencing of “perfect match” targets by miR* species depends on canonical siRNA pathway components.

miR* strands can silence targets *in vivo*

To test whether the miR* strands also function *in vivo*, we generated transgenic sensor flies in which binding sites for either strand of *miR-276a* or *miR-bantam* in perfect or bulged configurations were placed within the 3' UTR of an *EGFP* transgene. We tested silencing using

clonal analyses in the developing wing disc. In homozygous *dcr-1* clones, GFP signals from sensors for the miRNA strand of *miR-276a* or *miR-bantam* (in both perfect and bulged configurations) increased as expected (Fig. 6A,B; Supplementary Fig. 5A,B). Sensors for the miR* strand of *miR-bantam* (in perfect and bulged configurations) were also de-repressed in *dcr-1* clones (Fig. 6C,D). We did not observe the same effect with sensors for the *miR-276a** strand, presumably due to its low endogenous levels in the wing disc (Supplementary Fig. 5C,D). We conclude that the *miR-bantam** strand is generated in a Dcr-1-dependent manner and is capable of repressing sensors carrying either perfect or bulged binding sites.

In *ago1* clones, perfectly complementary sensors for the miR strand of *miR-276a* or *miR-bantam* were de-repressed (Fig. 6E; Supplementary Fig. 5E), as were sensors for the miR strand of *miR-276a* or *miR-bantam* in bulged configurations (Fig. 6F; Supplementary Fig. 5F). In *ago1*-mutant clones, we found that perfect match sensors for the miR* strand of *miR-bantam* became hyper-repressed as compared to background tissue, which is heterozygous for the *ago1* mutation. We saw concomitant de-repression in the twin spots, which carry two copies of the wild-type *ago1* gene (Fig. 6G). The increase in silencing upon AGO1 depletion is consistent with effects of *ago1* knockdown in S2 cells (Fig. 5, B-E). We were unable to detect significant de-repression of the sensors for the miR* strand of either *miR-bantam* or *miR-276a* in perfect configuration in *ago2* clones, possibly due to residual AGO2 protein in mutant clones (Supplementary Fig. 6). In fact, a sensor transgene for *esi-2.1*, a highly abundant endo-siRNA shown to be loaded to AGO2, was only mildly de-repressed in *ago2* clones (Supplementary Fig. 10). Neither were obvious phenotypes observed in *loqs* clones (Supplementary Fig. 9). We did observe a moderate de-repression of a perfect match sensor for the *miR-bantam** strand in *dcr-2* or *r2d2* clones (Supplementary Fig. 7G, 8G), consistent with their de-repression following similar treatment of S2 cells (Fig. 5B-E).

Thermodynamic properties of endo-siRNAs and strand selection

Our data indicated that central bulges are the major determinant of sorting and strand selection in mismatch-containing duplexes. For these species, the thermodynamic properties of duplex ends impact sorting and strand selection to only a minor degree. To test the contribution of thermodynamic asymmetry for sorting and loading from perfect duplexes, we analyzed the energies of endo-siRNAs from the *klarsicht* locus and of viral siRNAs. These were almost absent from AGO1 immunoprecipitates but were loaded into AGO2 (Fig. 2A). Only sequences where both the guide and passenger strands were cloned in libraries from AGO2 immunoprecipitates were considered for our analysis. We split siRNA duplexes into those showing strong asymmetry (strand bias of guide to passenger of 20:1 or higher) and weak asymmetry (strand bias of 5:1 or lower). We calculated the average thermodynamic energies of both ends considering up to six terminal nucleotides. The average energies of guide strand ends were divided by the average energies of passenger strand end and the results plotted (Fig. 7A). Endo-siRNAs derived from the *klarsicht* locus that show stronger asymmetry (as indicated by the ratio of 20:1 or higher) also show prominent differences in the end energy between guide and passenger strands for up to four terminal nucleotides. In contrast, *klarsicht* endo-siRNAs with low asymmetry (ratio of 5:1 or lower) show little if any energy differences between their ends. Similar results were obtained for siRNAs derived from viruses, although the magnitude of the overall energy differences was lower (Fig. 7A).

Discussion

MicroRNAs have been honed by evolution to selectively load one strand, the miR strand, into RISC and thus specifically regulate a set of targets that contain complementarity to its specific seed (Bushati and Cohen, 2007; Eulalio et al., 2008). The data presented herein suggest that

microRNA precursors can be bifunctional with individual strands adopting different fates within small RNA pathways. We find that miR* strands are not mere by-products of microRNA biogenesis but can instead be loaded into demonstrably functional AGO complexes. Notably, this occurs despite miR and miR* strands being produced by precisely the same biogenesis mechanism involving Drosha/Pasha and Dcr-1/Loqs-PB complexes (Fig. 4A). Current models incorporate coupled small RNA biogenesis and AGO loading in which Dicer-AGO interactions capture the energy of phosphodiester bond hydrolysis to facilitate incorporation of the small RNA into RISC. Results presented here seem at odds with this model unless Dcr-1 interacts simultaneously with AGO1 and AGO2 to drive the individual strands of a single duplex into separate RISCs. However, this seems unlikely because depletion of either AGO tends to enrich, rather than simultaneously deplete, those RNAs present within the other complex. miR* strands persist but lose their terminal 2'-O-methylation in the absence of Dcr-2/R2D2, and the ratio of miR*/miR of AGO2-bound small RNA species significantly decreases under these conditions, indicating that this complex is required not for biogenesis but instead for successful and proper miR* loading into AGO2. Thus, we instead favor a model in which the miR:miR* duplex is released from Dcr-1 and subsequently recognized by Dcr-2/R2D2 which shepherds loading into AGO2 (Fig. 7B). This release and rebinding has previously been proposed for strand selection within the siRNA pathway (Preall et al., 2006; Tomari and Zamore, 2005). Whether the proximate Dcr-1 product is ever released en route to miR strand loading into AGO1 remains an open question. In one scenario, loading of the miR strand could remain coupled to Dcr-1 cleavage with those duplexes destined to produce miR*/AGO2 RISC being produced and released by Dcr-1 enzymes that had not formed a complex with AGO1 prior to pre-miRNA cleavage. However, even Dcr-1 complexes must somehow coordinate loading of miR strands, which lie on either the 5p or 3p arm of the precursor, perhaps suggesting that the AGO1 loading machinery might also rely on Dcr-1 product release prior to loading so that both strands can be interrogated. This is further supported by the observation that the endo-siRNA *esi-2.3*, a Dcr-2 product, is preferentially loaded into AGO1 (Fig. 2B).

In this regard, several lines of evidence suggest that the availability of AGO proteins influences the fate of the miR and miR* strands. The absence of AGO1 clearly impacts the abundance of miR* strands relative to other small RNAs, e.g., endo-siRNAs, that join AGO2 complexes. However, the strongest indications for coupling between AGOs and the fates of miR and miR* come from functional analysis of sensors in cell culture and in animals. A comparison of tissues containing zero, one, or two copies of the *ago1* gene show a graded ability to repress sensors for the miR* strands of *miR-bantam* or *miR-276a*. As compared to heterozygous cells, homozygous *ago1* clones hyper-repress miR* sensors, while cells with two copies of intact *ago1* show reduced repression as compared to heterozygous cells. Thus, either a true coupling remains between the biogenesis machinery and AGO proteins that determines the fate of small RNA duplexes or the relative levels of proteins that will accept miR or miR* strands simply influence the availability of substrates for loading along each pathway.

Results presented herein incorporate several previously proposed rules for small RNA sorting in the *Drosophila* RNAi pathway but refine some and place these within an overall hierarchy for selection of both the loaded strand and the destination AGO protein. For imperfect small RNA duplexes, the principal determinant seems to be the detection of paired or unpaired residues around the ninth position of the interrogated strand. Each strand of a precursor duplex seems to be assessed individually, since a single microRNA precursor can funnel one strand into AGO1 with the other independently flowing into AGO2. This is not specific to small RNAs generated by Dcr-1, since endo-siRNAs, which are Dcr-2 products, also follow this rule and can, based upon the pattern of interior bulges, select a particular strand for loading into AGO1. Analyses of natural microRNAs and of experimentally altered precursor duplexes indicate that this strand selection rule dominates thermodynamic asymmetry. For example a number of miR* strands join AGO2 despite having a substantially more stable 5' end than the miR strand.

Previously proposed thermodynamic asymmetry rules (Khvorova et al., 2003; Schwarz et al., 2003) become dominant for perfectly paired small RNA duplexes, such as those arising from the *klarsicht* locus and from viruses. Thus our studies not only begin to hierarchically integrate rules for small RNA selection in the RNAi pathway, but also suggest that the pathways leading to the generation of miR-loaded AGO1 RISC and siRNA-loaded AGO2 RISC are perhaps not as separate as generally supposed.

Experimental Procedures

Cell culture, transfection, and RNAi

S2-NP cells were maintained, transfected and selected as previously described (see Supplementary Methods).

DNA constructs

DNA fragments (~500 bp) encompassing *miR-bantam* and *miR-276a* were amplified by PCR and cloned into pRmHa-3. Pairs of oligonucleotides containing three perfect or bulged target sites for *miR-bantam*, *miR-bantam**, *miR-276a* or *miR-276a** were annealed and cloned into pRmHa-3-*Renilla* or pJB8 (*tubulin-EGFP* in pCaSpeR4) to generate sensor constructs. A pair of oligonucleotides containing two perfect sites for *esi-2.1* was annealed and cloned into pJB8 to generate an *esi-2.1* sensor. All these sensor constructs were used to generate transgenic flies using standard *P*-element-mediated transformation. See Table S1 for oligonucleotide sequences.

β -elimination

The chemical structure of 3' termini of small RNAs was analyzed as described (Vagin et al., 2006) (see Supplementary Methods).

Immunoprecipitation

Cell extracts were prepared, evenly split and subjected to immunoprecipitation using antibodies against AGO1 (Abcam) or the FLAG epitope (Sigma), respectively, as described (Czech et al., 2008; Zhou et al., 2008). RNAs were recovered from the immunoprecipitated samples using TRIzol (Invitrogen) and used for production of small RNA libraries or Northern blotting.

Northern Blotting

Northern blotting was carried out as described (Czech et al., 2008; Zhou et al., 2009) (see Supplementary Methods).

Small RNA libraries

Small RNAs were cloned as described (Brennecke et al., 2007). A detailed description of small RNA libraries prepared or used in this study can be found at the Supplementary Methods.

Bioinformatic analysis of small RNA libraries

The analysis of small RNA libraries was performed similar as described (Czech et al., 2008) (see Supplementary Methods).

Fly strains

Fly strains were maintained in standard media. All generated and used strains are listed in Table S2.

Clonal analysis

Clonal analysis was performed as described (Brennecke et al., 2005). Briefly, developing larva were heat-shocked at 37°C for one hour at 50-60 hours of development for flies carrying mutations for *dcr-1*, *dcr-2*, *ago2*, *r2d2* or *loqs* except for *ago1* flies, which were heat-shocked at 96-108 hours of development. Wandering third-instar larva were dissected and the imaginal wing discs were fixed in 4% formaldehyde-PBS at room temperature for 30 minutes, stained with monoclonal anti-β-Gal antibody (1:500; Promega), rabbit anti-GFP antibody (1:1000; Molecular Probes), and secondary antibodies (Alexa 488-conjugated goat anti-rabbit and Alexa 594-conjugated goat anti-mouse; 1:500; Molecular Probes). A rat anti-HA antibody (1:1000; Roche) was employed to examine the expression pattern of FLAG/HA-AGO2 in the imaginal wing disc.

Argonaute loading assay

Cells expressing FLAG/HA-AGO2 (see above) were transfected with various siRNA or miRNA duplexes (Table S1) using HiPerfect (Qiagen). Two days after transfection, cell lysates were prepared, evenly split, and each half subjected to immunoprecipitation using antibodies against AGO1 and the FLAG-tag respectively (see above). RNAs were recovered from the immunoprecipitates and subjected to sequential Northern blotting using a mixture of probes complementary to the top strands or to the bottom strands of the *miR-276a* or *let-7* series of duplexes, and those against *miR-bantam* and the guide strand of *esi-2.1*. The intensity of the signals was quantified and normalized to those of *esi-2.1* and *miR-bantam* for AGO2 and AGO1 loading, respectively. The corresponding Argonaute loading index for each sample was calculated using the following equation. For example, the AGO1 loading index for the top strand of *miR-276a* duplex 1 is calculated as:
$$\frac{[(miR-276a \text{ duplex \#1 top strand } miR-276a \text{ duplex \#1 tfxn AGO1 IP-gel background}) / (miR-bantam \text{ } miR-276a \text{ duplex \#1 tfxn AGO1 IP-gel background})] - [(miR-276a \text{ duplex \#1 top strand non-transfection control AGO1 IP-gel background}) / (miR-bantam \text{ non-transfection control AGO1 IP-gel background})]}{}$$
 To calculate the relative Argonaute loading index, the $\frac{AGO1 \text{ index}}{AGO2 \text{ index}}$ ratio for each strand of the duplex was determined. Finally, the relative Argonaute index for each strand was normalized to that of the corresponding strand of duplex 1, and the results were \log_2 transformed and plotted.

Thermodynamics calculations

All 21-nt long reads within the wild-type AGO2 IP library matching to the *klarsicht* locus or viral genomes were extracted bioinformatically (Czech et al., 2008). Only those sequences corresponding to pairs of guide and passenger strands resembling perfect match duplexes with 2-nt overhangs at the 3' termini were subjected to further analysis. The terminal energies of up to six nucleotides counted from both ends those duplexes were calculated individually using UNAFold (Markham and Zuker, 2008). Sequences matching to both categories were next grouped into strong asymmetric duplexes (cloning count ratio of guide to passenger of 20:1 or higher) and weak asymmetric duplexes (strand bias of 5:1 or less). Average energies were computed for both groups and energies of guide strand ends were divided by energies for passenger strand ends. To correlate the energies with the degree of asymmetry, the median results were plotted for all six nucleotides individually.

Supplementary Material

Refer to Web version on PubMed Central for supplementary material.

Acknowledgments

We thank R. Carthew, Q. Liu, P. Jin, H. Siomi, P.D. Zamore, E. Lai, and the Bloomington Stock Center for fly strains. We are grateful to M. Kudla, O. Tam, M. Rooks, D. McCombie, and C. Pitsouli for technical and computational contributions. We thank R. Davis and J. Dover for kindly sequencing two Solexa libraries at University of Colorado, Denver. B.C. is supported by a PhD fellowship from the Boehringer Ingelheim Fonds. R.Z. is a Special Fellow of the Leukemia and Lymphoma Society. This work was supported in part by grants from the NIH to N.P. and G.J.H. and a gift from K. W. Davis (G.J.H.). N.P. and G.J.H. are investigators of the HHMI. Small RNA sequences generated in this study can be obtained at GEO using accession number GSE17734.

References

- Aliyari R, Wu Q, Li HW, Wang XH, Li F, Green LD, Han CS, Li WX, Ding SW. Mechanism of induction and suppression of antiviral immunity directed by virus-derived small RNAs in *Drosophila*. *Cell Host Microbe* 2008;4:387–397. [PubMed: 18854242]
- Brennecke J, Aravin AA, Stark A, Dus M, Kellis M, Sachidanandam R, Hannon GJ. Discrete small RNA-generating loci as master regulators of transposon activity in *Drosophila*. *Cell* 2007;128:1089–1103. [PubMed: 17346786]
- Brennecke J, Stark A, Russell RB, Cohen SM. Principles of microRNA-target recognition. *PLoS Biol* 2005;3:e85. [PubMed: 15723116]
- Bushati N, Cohen SM. microRNA functions. *Annu Rev Cell Dev Biol* 2007;23:175–205. [PubMed: 17506695]
- Chung WJ, Okamura K, Martin R, Lai EC. Endogenous RNA interference provides a somatic defense against *Drosophila* transposons. *Curr Biol* 2008;18:795–802. [PubMed: 18501606]
- Czech B, Malone CD, Zhou R, Stark A, Schlingeheyde C, Dus M, Perrimon N, Kellis M, Wohlschlegel JA, Sachidanandam R, et al. An endogenous small interfering RNA pathway in *Drosophila*. *Nature* 2008;453:798–802. [PubMed: 18463631]
- Denli AM, Tops BB, Plasterk RH, Ketting RF, Hannon GJ. Processing of primary microRNAs by the Microprocessor complex. *Nature* 2004;432:231–235. [PubMed: 15531879]
- Eulalio A, Huntzinger E, Izaurralde E. Getting to the root of miRNA-mediated gene silencing. *Cell* 2008;132:9–14. [PubMed: 18191211]
- Flynt A, Liu N, Martin R, Lai EC. Dicing of viral replication intermediates during silencing of latent *Drosophila* viruses. *Proc Natl Acad Sci U S A* 2009;106:5270–5275. [PubMed: 19251644]
- Forstemann K, Horwich MD, Wee L, Tomari Y, Zamore PD. *Drosophila* microRNAs are sorted into functionally distinct argonaute complexes after production by dicer-1. *Cell* 2007;130:287–297. [PubMed: 17662943]
- Forstemann K, Tomari Y, Du T, Vagin VV, Denli AM, Bratu DP, Klattenhoff C, Theurkauf WE, Zamore PD. Normal microRNA maturation and germ-line stem cell maintenance requires Loquacious, a double-stranded RNA-binding domain protein. *PLoS Biol* 2005;3:e236. [PubMed: 15918770]
- Ghildiyal M, Seitz H, Horwich MD, Li C, Du T, Lee S, Xu J, Kittler EL, Zapp ML, Weng Z, Zamore PD. Endogenous siRNAs derived from transposons and mRNAs in *Drosophila* somatic cells. *Science* 2008;320:1077–1081. [PubMed: 18403677]
- Gregory RI, Yan KP, Amuthan G, Chendrimada T, Doratotaj B, Cooch N, Shiekhattar R. The Microprocessor complex mediates the genesis of microRNAs. *Nature* 2004;432:235–240. [PubMed: 15531877]
- Hammond SM, Bernstein E, Beach D, Hannon GJ. An RNA-directed nuclease mediates post-transcriptional gene silencing in *Drosophila* cells. *Nature* 2000;404:293–296. [PubMed: 10749213]
- Hartig JV, Esslinger S, Bottcher R, Saito K, Forstemann K. Endo-siRNAs depend on a new isoform of loquacious and target artificially introduced, high-copy sequences. *EMBO J*. 2009
- Horwich MD, Li C, Matranga C, Vagin V, Farley G, Wang P, Zamore PD. The *Drosophila* RNA methyltransferase, DmHen1, modifies germline piRNAs and single-stranded siRNAs in RISC. *Curr Biol* 2007;17:1265–1272. [PubMed: 17604629]
- Iwasaki S, Kawamata T, Tomari Y. *Drosophila* argonaute1 and argonaute2 employ distinct mechanisms for translational repression. *Mol Cell* 2009;34:58–67. [PubMed: 19268617]

- Jiang F, Ye X, Liu X, Fincher L, McKearin D, Liu Q. Dicer-1 and R3D1-L catalyze microRNA maturation in *Drosophila*. *Genes Dev* 2005;19:1674–1679. [PubMed: 15985611]
- Kawamura Y, Saito K, Kin T, Ono Y, Asai K, Sunohara T, Okada TN, Siomi MC, Siomi H. *Drosophila* endogenous small RNAs bind to Argonaute 2 in somatic cells. *Nature* 2008;453:793–797. [PubMed: 18463636]
- Khorova A, Reynolds A, Jayasena SD. Functional siRNAs and miRNAs exhibit strand bias. *Cell* 2003;115:209–216. [PubMed: 14567918]
- Lee Y, Ahn C, Han J, Choi H, Kim J, Yim J, Lee J, Provost P, Radmark O, Kim S, Kim VN. The nuclear RNase III Droscha initiates microRNA processing. *Nature* 2003;425:415–419. [PubMed: 14508493]
- Lee Y, Kim M, Han J, Yeom KH, Lee S, Baek SH, Kim VN. MicroRNA genes are transcribed by RNA polymerase II. *EMBO J* 2004a;23:4051–4060. [PubMed: 15372072]
- Lee YS, Nakahara K, Pham JW, Kim K, He Z, Sontheimer EJ, Carthew RW. Distinct roles for *Drosophila* Dicer-1 and Dicer-2 in the siRNA/miRNA silencing pathways. *Cell* 2004b;117:69–81. [PubMed: 15066283]
- Liu Q, Rand TA, Kalidas S, Du F, Kim HE, Smith DP, Wang X. R2D2, a bridge between the initiation and effector steps of the *Drosophila* RNAi pathway. *Science* 2003;301:1921–1925. [PubMed: 14512631]
- Markham NR, Zuker M. UNAFold: software for nucleic acid folding and hybridization. *Methods Mol Biol* 2008;453:3–31. [PubMed: 18712296]
- Matranga C, Tomari Y, Shin C, Bartel DP, Zamore PD. Passenger-strand cleavage facilitates assembly of siRNA into Ago2-containing RNAi enzyme complexes. *Cell* 2005;123:607–620. [PubMed: 16271386]
- Miyoshi K, Tsukumo H, Nagami T, Siomi H, Siomi MC. Slicer function of *Drosophila* Argonautes and its involvement in RISC formation. *Genes Dev* 2005;19:2837–2848. [PubMed: 16287716]
- Okamura K, Chung WJ, Ruby JG, Guo H, Bartel DP, Lai EC. The *Drosophila* hairpin RNA pathway generates endogenous short interfering RNAs. *Nature* 2008a;453:803–806. [PubMed: 18463630]
- Okamura K, Phillips MD, Tyler DM, Duan H, Chou YT, Lai EC. The regulatory activity of microRNA* species has substantial influence on microRNA and 3' UTR evolution. *Nat Struct Mol Biol* 2008b;15:354–363. [PubMed: 18376413]
- Park JK, Liu X, Strauss TJ, McKearin DM, Liu Q. The miRNA pathway intrinsically controls self-renewal of *Drosophila* germline stem cells. *Curr Biol* 2007;17:533–538. [PubMed: 17320391]
- Preall JB, He Z, Gorra JM, Sontheimer EJ. Short interfering RNA strand selection is independent of dsRNA processing polarity during RNAi in *Drosophila*. *Curr Biol* 2006;16:530–535. [PubMed: 16527750]
- Saito K, Ishizuka A, Siomi H, Siomi MC. Processing of pre-microRNAs by the Dicer-1-Loquacious complex in *Drosophila* cells. *PLoS Biol* 2005;3:e235. [PubMed: 15918769]
- Saito K, Sakaguchi Y, Suzuki T, Siomi H, Siomi MC. Pimet, the *Drosophila* homolog of HEN1, mediates 2'-O-methylation of Piwi-interacting RNAs at their 3' ends. *Genes Dev* 2007;21:1603–1608. [PubMed: 17606638]
- Schwarz DS, Hutvagner G, Du T, Xu Z, Aronin N, Zamore PD. Asymmetry in the assembly of the RNAi enzyme complex. *Cell* 2003;115:199–208. [PubMed: 14567917]
- Seitz H, Ghildiyal M, Zamore PD. Argonaute loading improves the 5' precision of both MicroRNAs and their miRNA strands in flies. *Curr Biol* 2008;18:147–151. [PubMed: 18207740]
- Tomari Y, Du T, Zamore PD. Sorting of *Drosophila* small silencing RNAs. *Cell* 2007;130:299–308. [PubMed: 17662944]
- Tomari Y, Matranga C, Haley B, Martinez N, Zamore PD. A protein sensor for siRNA asymmetry. *Science* 2004;306:1377–1380. [PubMed: 15550672]
- Tomari Y, Zamore PD. Perspective: machines for RNAi. *Genes Dev* 2005;19:517–529. [PubMed: 15741316]
- Vagin VV, Sigova A, Li C, Seitz H, Gvozdev V, Zamore PD. A distinct small RNA pathway silences selfish genetic elements in the germline. *Science* 2006;313:320–324. [PubMed: 16809489]
- Zhou R, Czech B, Brennecke J, Sachidanandam R, Wohlschlegel JA, Perrimon N, Hannon GJ. Processing of *Drosophila* endo-siRNAs depends on a specific Loquacious isoform. *RNA*. 2009

Zhou R, Hotta I, Denli AM, Hong P, Perrimon N, Hannon GJ. Comparative analysis of argonaute-dependent small RNA pathways in *Drosophila*. *Mol Cell* 2008;32:592–599. [PubMed: 19026789]

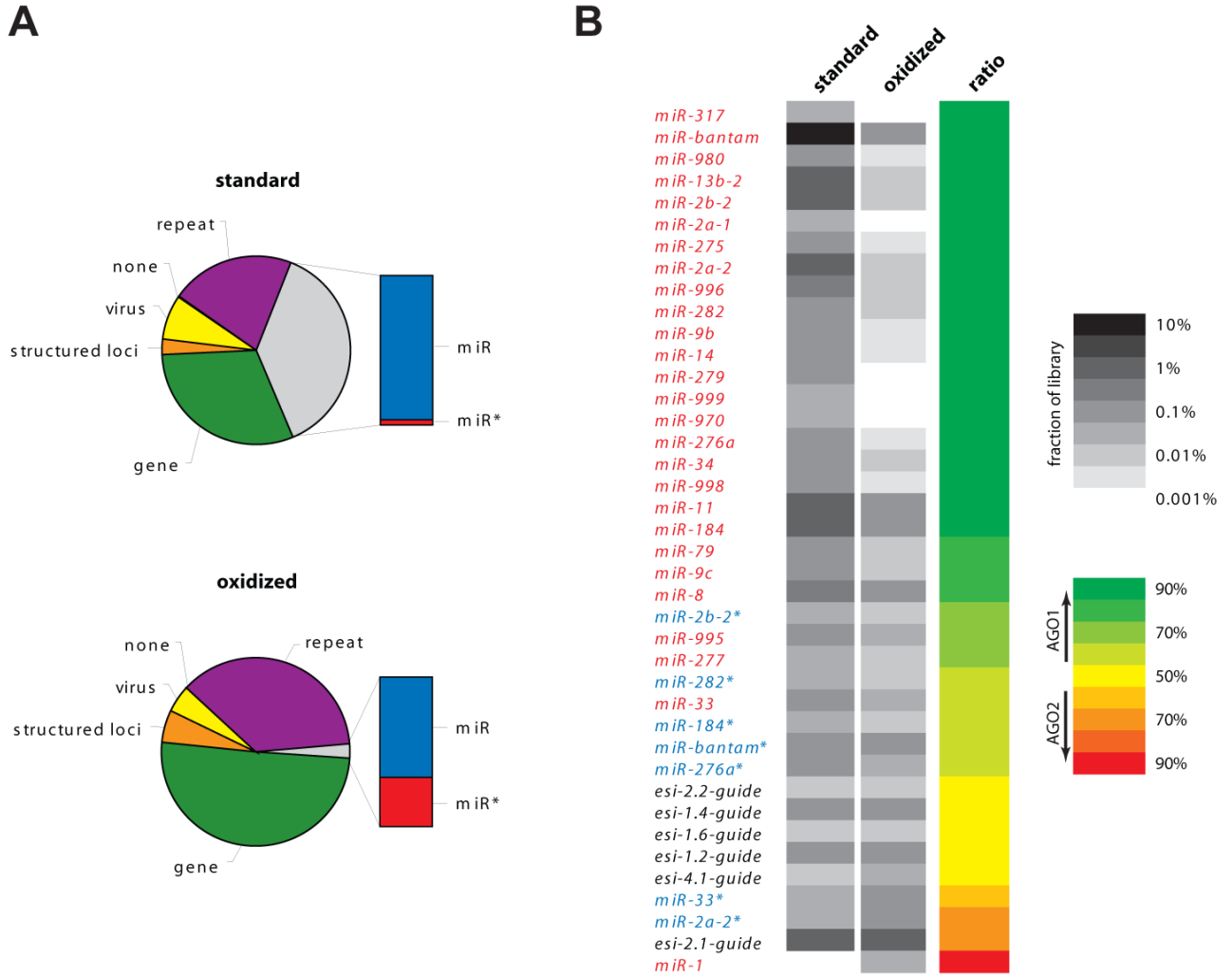


Figure 1. miR*s have modified 3' termini

(A) Pie charts represent the relative abundance of different endo-siRNA classes and microRNAs in 19- to 24-nt small RNA libraries from wild-type S2 cells. Results from a standard cloning protocol (upper diagram) and from a cloning strategy that enriches for small RNAs with modified 3' termini (lower diagram) are shown. The fraction of miRs and miR*s is indicated for both libraries. (B) Heatmaps show the relative abundance of endo-siRNAs derived from structured loci, miRs, and miR*s in the indicated libraries (in grayscale). The ratio of normalized representation in the libraries indicates preferential association of small RNAs with either AGO1 (green) or AGO2 (red).

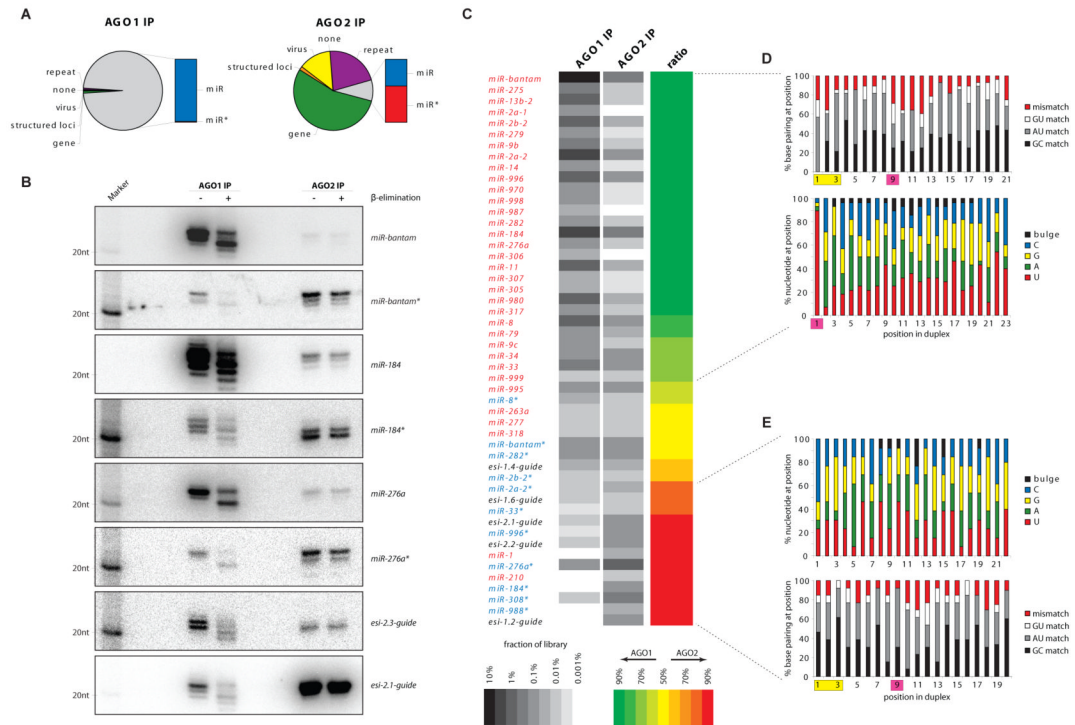


Figure 2. miR*s are preferentially loaded into AGO2

(A) Pie charts show the relative abundance of endo-siRNA classes and microRNAs libraries from AGO1 (left diagram) and AGO2 (right diagram) immunoprecipitates from S2 cells. (B) Northern blots of RNA from AGO1 and AGO2 immunoprecipitates from S2 cells. AGO-bound small RNAs were untreated (–) or subjected to β-elimination (+) prior to gel electrophoresis. The same membrane was probed for three miRNAs, three miR*s, and two endo-siRNAs derived from structured loci. (C) Heatmaps showing the relative abundance of endo-siRNAs derived from structured loci, miRNAs and miR*s in AGO1 and AGO2 libraries (grayscale). The relative association of small RNAs with AGO1 or AGO2 is indicated on a red/green scale. (D) Median base pairing (upper chart) and nucleotide composition (lower chart) of all sequences that show a relative association with AGO1 of 70% or more. Bulges on each strand were counted as mismatches (E) Analysis as in (D) but with all sequences having a relative association of 70% or more with AGO2.

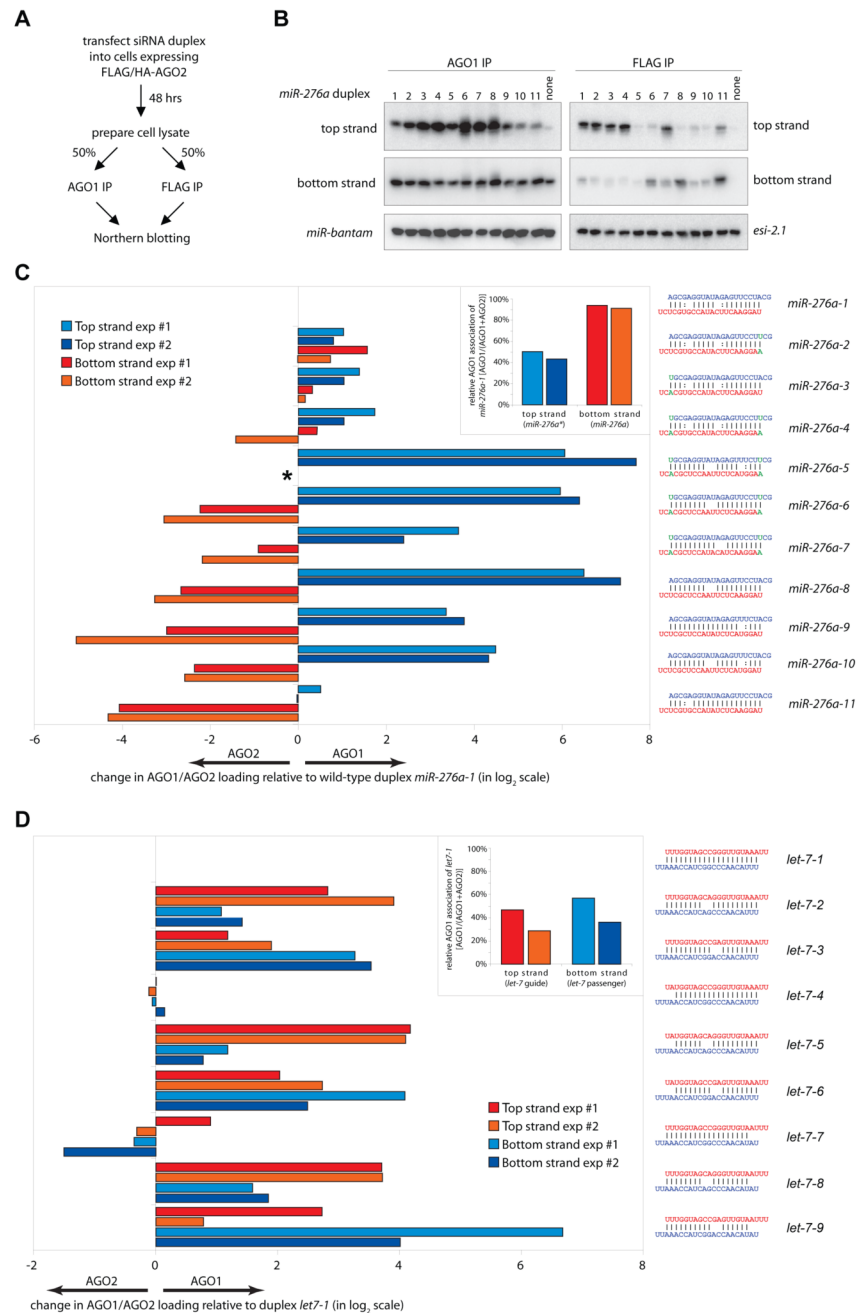


Figure 3. Small RNA duplexes can be directed to AGO1 or AGO2
(A) Schematic drawing of the experimental procedure (Argonaute loading assay). **(B)** Immunoprecipitation followed by Northern blotting shows the loading of both top and bottom strands of various modified *miR-276a* duplexes into AGO1 or AGO2. *miR-bantam* and *esi-2.1* served as controls. **(C)** Quantification of the Argonaute loading assay for modified *miR-276a* duplexes. The relative Argonaute loading index for each strand was normalized to that of the corresponding strand of duplex #1 (wild-type control), results were log₂ transformed and plotted. Positive numbers indicate preferential loading into AGO1, whereas negative numbers indicate favored loading into AGO2. The asterisk indicates that the bottom strand of duplex 5 had low signal and could not be reliably quantified. The inset shows the

loading pattern of both individual strands of duplex #1. Duplex structures are shown to the right. **(D)** The relative Argonaute loading index for modified *let-7* duplexes as described in **(C)**.

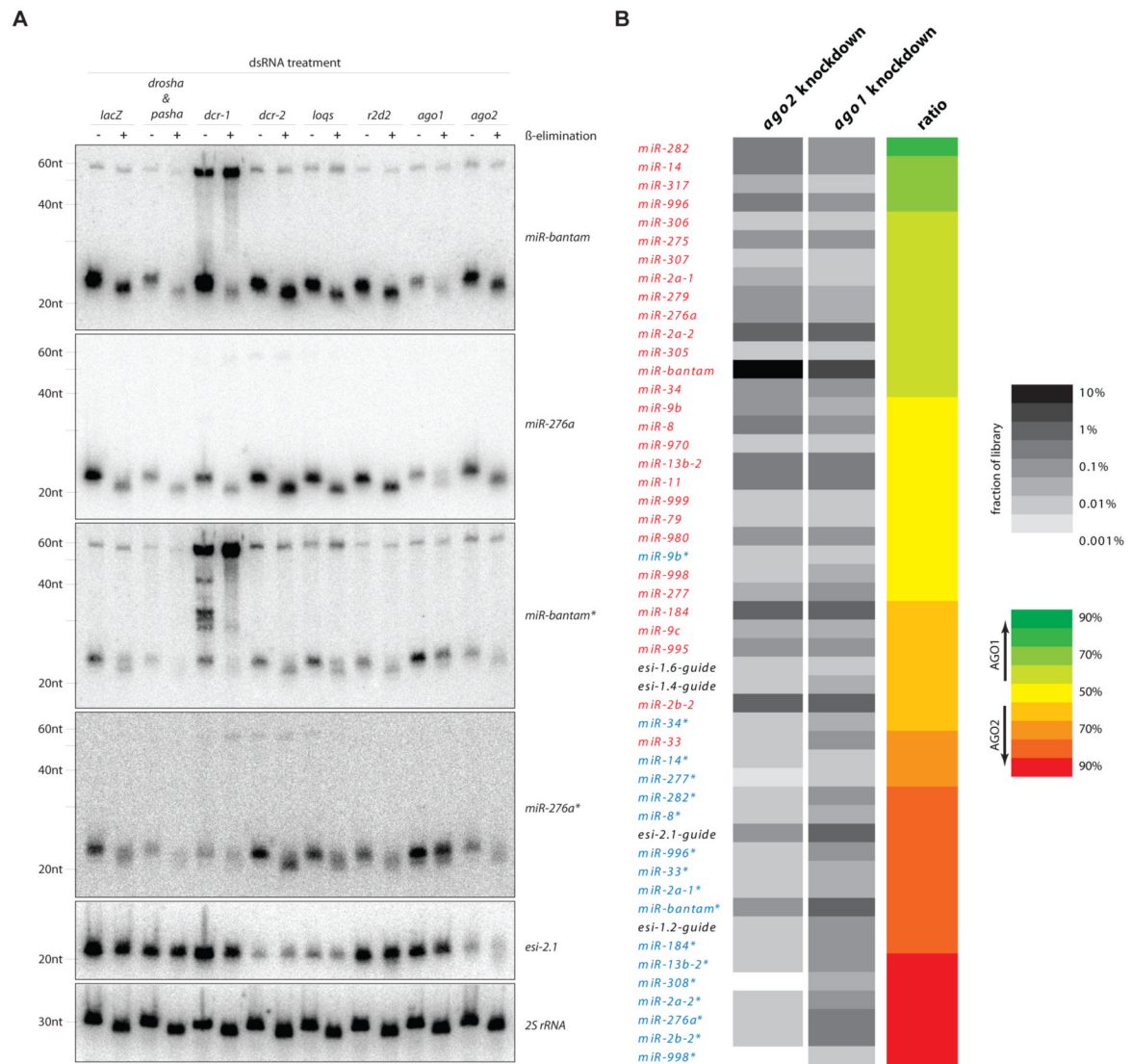


Figure 4. Requirements for biogenesis and loading of miR*s

(A) Northern blots were probed with two miRs, two miR*s, and an endo-siRNA derived from a structured locus. Total RNAs from the indicated RNAi knockdowns were untreated (–) or subjected to β-elimination (+) prior to gel electrophoresis. 2S rRNA served as loading control. (B) Heatmaps showing the relative abundance of miRs, miR*s, and endo-siRNAs derived from structured loci in total RNA libraries of samples treated with dsRNAs against AGO1 or AGO2 (in grayscale). Preferential dependence of small RNAs on AGO1 (green) or AGO2 (red) is shown to the right.

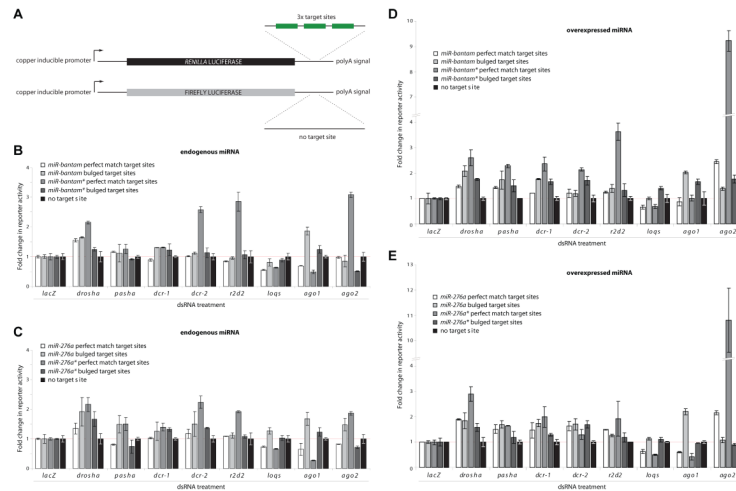


Figure 5. Silencing by miR and miR* strands in S2 cells

(A) Schematic diagram showing the configuration of the sensor constructs. Three perfect match or bulged target sites for the miR or miR* strands of *miR-bantam* and *miR-276a* were placed in the 3' UTR of the *Renilla* luciferase gene. A firefly luciferase construct without target sites served as a normalization control. (B) The indicated *Renilla* luciferase sensor constructs for *miR-bantam* or a control *Renilla* luciferase construct without target sites were co-transfected into S2 cells with a firefly luciferase construct. Cells were treated with dsRNAs targeting indicated RNAi pathway components. Fold changes in reporter activity were calculated as *Renilla*/firefly ratio normalized first against the control sample (cells treated with dsRNA targeting *lacZ*), then against cells transfected with the control construct without target sites. Shown is the average reporter activity with standard deviation (n=2). (C) Sensor activities for *miR-276a* as described in (B). (D) Sensor activities for over-expressed *miR-bantam*. Experiments were performed as described in (B) but in addition, an expression construct for *miR-bantam* was co-transfected with the reporter constructs. (E) Sensor activities for over-expressed *miR-276a* as described in (D).

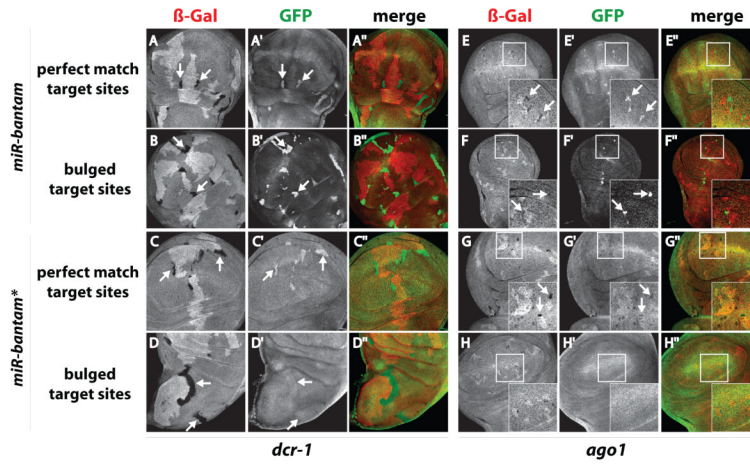


Figure 6. Silencing by miR and miR* strands in flies

Shown are sensors for *miR-bantam* or *miR-bantam** containing perfectly matched or bulged target sites (as indicated to the left). (**A-D**). β -Gal staining (red in the merged images) indicates *dcr-1* mutant clones (also marked with arrows). Cells with strong β -Gal staining contain two wild-type *dcr-1* genes, while cells with intermediate staining are heterozygous for *dcr-1*. EGFP sensor activity is shown in green. The black and white panels indicate the separate channels for β -Gal and EGFP. (**E-H**) Clonal analysis for *ago1*: Details as in (**A-D**). Selected regions (enclosed in white boxes) were enlarged and shown as insets within each panel to display the smaller *ago1* clones.

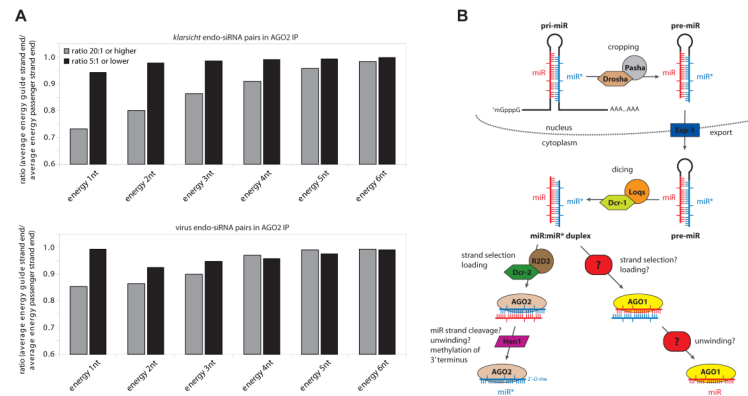


Figure 7. A hierarchy of rules for small RNA loading in flies

(A) Thermodynamic properties of AGO2-associated endo-siRNAs matching the *klarsicht* locus (upper chart) and viral siRNAs (lower chart). All siRNA duplexes with both strands cloned were extracted bioinformatically and ratios of cloning abundances between guide and passenger strands were calculated. Average energies for up to six terminal nucleotides were plotted for strongly asymmetric (strand bias of 20:1 or higher) and weakly asymmetric duplexes (strand bias of 5:1 or lower). **(B)** Model for differential sorting of miRNA duplexes in flies.